# Electrospun Ultrafine Composite Fibers from Organic-Soluble Chitosan and Poly(ethylene oxide)

Wenkai Chang,[1] Guiping Ma,[1] Dongzhi Yang,[1] Dandan Su,[1] Guoqiang Song,[2] Jun Nie[1]

[1]State Key Laboratory of Chemical Resource Engineering, Beijing University of Chemical Technology, Beijing 100029, People's Republic of China
[2]Department of Chemical Engineering, Jiangsu Polytechnic University, Changzhou 213164, Jiangsu, People's Republic of China

**ABSTRACT:** The ultrafine composite fibers had been successfully achieved by electrospinning of chloroform solutions of octadecyl chitosan (O-CS) and poly(ethylene oxide) (PEO). The ultrafine composite fibers membranes were subjected to detailed analysis by Fourier-transformed infrared spectroscopy (FTIR), scanning electron microscopy (SEM), and water contact angle (WCA). The FTIR results confirmed that ultrafine composite fibers contained the two polymers. The SEM images showed that the morphology and diameter of the composite fibers were mainly affected by the weight ratio of O-CS/PEO, the electric field strength, and the collection distance. The WCA data demonstrated that the composite fibers membranes performed a quite hydrophobic character. The special morphology of neck and porous structure was observed experimentally during electrospinning. The neck structure was due to the fibers elongated in the direction of stretching through the electric field, and the porous structure was decided by the competition between the phase separation and the fast evaporation rate of chloroform. © 2010 Wiley Periodicals, Inc. J Appl Polym Sci 117: 2113–2120, 2010

**Key words:** organic-soluble chitosan; poly(ethylene oxide); electrospinning; composite fibers; water contact angle

## INTRODUCTION

The ultrafine fiber materials from biodegradable and biocompatible synthetic and/or natural polymers are drawing great interest because of their unique properties. It has been put into the areas of biomedicine, pharmaceuticals, cosmetics, and food science.[1] Electrospinning is a promising technique for producing continuous polymer fibers with diameters ranged from 5 to 500 nm, yielding three-dimensional fibers with a large specific surface area,[2,3] using the action of an external electric field imposed on a polymer solution or melt.[4] In comparison to conventional fibers processing methodologies, such as fibers drawing and rotating disc techniques,[5,6] electrospinning has been shown to produce much finer fibers. Because of the rapid evaporation and simultaneously superimposed mechanical stresses due to developing bending instabilities of the polymer jet, polymers in electrospun fibers are more oriented than the original polymer and therefore exhibit better mechanical

properties and higher thermal stability.[7–9] With the high-specific surface area and small porous size, polymer ultrafine fibers can be used as filter materials, sensors, wound dressings, controlled release carriers, and tissue engineering scaffolds.[10–12] The morphology and diameters of electrospun fibers depend on a number of parameters, which include properties and composition of the spinning solution such as polymer type, conformation of polymer chain, viscosity of the solution, conductivity, polarity, and surface tension of solvent; electrospinning conditions such as applied field strength, distance between the capillary and collector, and feeding rate.[13–15] By proper selection of system and process parameters, electrospun fibers with varied morphology can be obtain.

Much attention has been focused on the electrospinning of chitosan recently. Among polysaccharides, chitosan is produced from a N-deacetylation of chitin which is one of the second most abundant polysaccharides commonly found in shells of various insects and crustaceans as well as cell walls of various fungal in alkaline conditions.[16] Chitosan is widely used in pharmaceutical and biomedical fields for its biodegradable and biocompatibility: for cells encapsulation,[17] drug delivery,[18] cell culture,[19] hyaline cartilage repairs,[20] and bone reconstruction.[21] Electrospinning of two or several biopolymers has become an advanced technique to develop new

biomaterials possessed many properties that could not be obtained by individual polymers. There are much research on the composite fibers of chitosan and another polymer such as polyvinylalcohol, poly-acrylonitrile, and silk fibroin in the organic or acids solutions.[22–25] Unfortunately, its utilization is limited by its poor solubility and reactivity, a direct result of strong intra- and intermolecular hydrogen bonding. It seems more difficult to produce biomacromolecular composite fibers due to their limited solubility to most organic solvents, ionic character in dissolved state and three-dimensional networks of strong hydrogen bonds. However, the presence of amino group could be modified by controlled chemical reactions. An approach is chemical modifications of chitosan into derivatives that are soluble in a wide variety of common organic solvents. Organic soluble derivatives of chitosan can be used to formulate materials for biomedical applications such as polymeric drugs and artificial organs with high specificity and wide applicability. Among such derivatives, acylated chitosan are soluble in various common organic solvents, such as chloroform, benzene, pyridine, and tetrahydrofuran.[26]

Poly(ethylene oxide) (PEO), an amphiphilic (soluble both in polar and nonpolar solvents) and nondegradable polymer with good biocompatibility, is one of the few synthetic polymers approved for internal use in food, cosmetics, personal care products, and pharmaceutical. To produce ultrafine composite fibers of organic-soluble chitosan, PEO is added with different ratios to O-CS solutions to improve the electrospinnability and viscosity. PEO was selected for not only its production of ultrafine electrospun composite fibers but also its properties, which are similar to many polysaccharides such as a linear structure, capable of forming hydrogen bonds with other polymers.[23,27]

In this work, ultrafine composite fibers were fabricated by electrospinning of O-CS/PEO mixed solutions. The composite fibers were examined by Fourier-transformed infrared (FTIR) spectroscopy. The morphology, diameter distribution, and surface properties of the composite fibers were investigated by scanning electron microscope (SEM). The contact angles of O-CS/PEO composite fibers membrane against water were also measured in detail.

## EXPERIMENTAL SECTION

### Materials

Organic-soluble chitosan was prepared by acylation reaction of chitosan with octadecyl chloride based on the method described in our previous report.[28] Polyethylene oxide (PEO, $M_w = 900,000$) was purchased from Sumitomo Seika Chemicals (Osaka,

Japan). Chloroform and ethanol was used as received from Beijing Chemical Reagent Company (Beijing, China). All chemicals and reagents used were of analytical grade.

### Preparation of solutions for electrospinning

O-CS solution (8.0%, w/w) was prepared by dissolving 8.0 g O-CS into 91.2 g chloroform. Polyethylene oxide (PEO) solution (3.0%, w/w) was prepared by adding 3.0 g PEO powder into 96.2 g chloroform. Both the aforementioned solutions were added 0.8 g ethanol (0.8%, w/w) as a stabilizer of chloroform. The two solutions were stirred with magnetic stir for at least 24 h at room temperature. The electrospinning solutions of O-CS/PEO were prepared by mixing 8 wt % O-CS solution with 3 wt % PEO solution at O-CS/PEO weight ratios 1/3, 1/2, 1/1, 2/1, and 3/1. All of the experimental operation was completed at room temperature.

### Measurement of the viscosity

The apparent viscosity of polymer dispersions was determined by shear rheometry. The shear viscosity of different O-CS/PEO weight ratios mixed solution were independently determined at the shear rate of 340 s$^{-1}$ with a rotational viscometer (NDJ-79, Jichang Geology Instrument, Shanghai, China) equipped with coaxial cylinders at 25 °C. The reported value for each sample was obtained by averaging several repeated measurements.

### Electrospinning of ultrafine composite fibers

The electrospinning apparatus consisted of a syringe pump (KDS100, KD Scientific, Holliston, MA), a high-voltage generator (BMEI Co., Ltd., Beijing, China), and aluminum foils as targets for fibers collection. Electrospinning was performed with spinning configuration using a polytetrafluoroethylene (PTFE) capillary tube, its one head was connected to a disposable syringe filled with 5 mL of a O-CS/PEO blend solution, a constant volume flow rate was maintained by using a syringe pump, another head equipped with steel needle mounted in an adjustable, electrically insulated parallel plate geometry. An aluminum foil was used as the collector which electrospun fibers were deposited. The applied voltages were in the range from 4 to 30 kV, driven by a high-voltage power supply (BMEI, China). The electric potential, the solution flow rate, and the collection distance were adjusted so that a stable jet could obtain. In the electrospinning process, the pendant droplet at the syringe tip was split by a repulsion force provided by the charge in the surface of droplet, and formed a jet of a cone-like
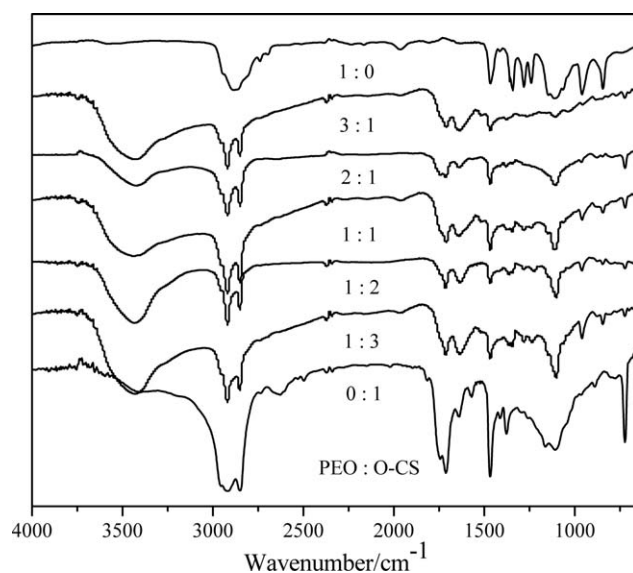
**Figure 1** FTIR spectra of electrospun ultrafine composite fibers with O-CS/PEO mass ratios of 0 : 1, 1 : 3, 1 : 2, 1 : 1, 2 : 1, 3 : 1, and 1 : 0.

shape when it was traveling toward the collection screen, then the solvent evaporated and polymer fibers deposited on the collection screen to form a nanofibers membrane.

## Fourier-transformed infrared spectroscopy

To determine composition and chemical characteristics of fibers, FTIR (Thermo Nicolet 5700, Thermo Nicolet Instrument Corp., Madison, WI) was used to analyze the absorbance in the wavenumber range of 650–4000 cm$^{-1}$ with a resolution of 4 cm$^{-1}$. The membrane was ground into fine powder, mixed with KBr powder (1 : 50), dried and compressed into pellets for FTIR examination.

## Scanning electron microscope

The morphology of prepared composite fibers was examined by using a SEM (S4700, Hitachi Ltd, Tokyo, Japan). Prior to imaging, the samples were sputter-coated with a gold layer 20–30 nm thick for better conductivity during imaging. The diameter and distributions of ultrafine composite fibers were measured by Image J analysis software.

## Water contact angle

The surface properties of composite fibers were characterized by studying the water contact angle (WCA) of produced electrospun membranes. WCA was measured at room temperature, using droplet drop method on a contact angle instrument (OCA 20, Dataphysics, Dilderstadt, Germany). The WCA value for each sample was obtained by averaging at

least 10 measurements on different positions of the surface. The volume of the water droplet for each measurement was kept at $2 \times 10^{-9}$ m$^3$.

## RESULTS AND DISCUSSION

### Fourier-transformed infrared spectroscopy

Figure 1 displayed the FTIR spectra of the ultrafine composite fibers of O-CS and PEO. The band positions and their assignments, identification are listed in Table I. For O-CS, the broad feature at 3440 cm$^{-1}$ attributed to the inter- and intramolecular hydrogen bonding of amine groups (NH$_2$) and hydroxyl groups (OH) stretching vibration, this indicated that acylation reaction did not fully substitute the hydroxyl and amine groups on chitosan molecules. Owing to the formation of hydrogen bonding between PEO and O-CS, the intensity of peak in the composite fibers was stronger than that in O-CS. The characteristic peaks at 1720 cm$^{-1}$ (C=O of NCOR) and 1751 cm$^{-1}$ (C=O of OCOR) were brought by the acylation reaction between octadecyl chloride and the groups (—NH$_2$, —OH) of chitosan. Other prominent peaks at 2920 cm$^{-1}$ and 2850 cm$^{-1}$ were assigned to the asymmetrical and symmetrical bending vibrations of CH$_2$ groups.

For PEO, the absorption peak at 2900 cm$^{-1}$ could be attributed to the molecular stretching of the CH$_2$ group, the peak at 1455 cm$^{-1}$ attributed to CH$_2$ bending, whereas peaks at 1100 and 958 cm$^{-1}$ were due to the stretching of the C—O—C group in PEO.[29–31] Each absorption peaks of O-CS and PEO were identified, except for variations in the intensity of some bands, no significant shifts were observed, which confirmed that every fibers membrane was composed of the two polymers.

### Scanning electron microscope

The SEM micrographs of the fibers obtained at different weight ratios were shown in Figure 2. The morphology of electrospun ultrafine composite fibers and the fibers diameters were strongly influenced by

**TABLE I**
**FTIR Data for O-CS/PEO Ultrafine Composite Fibers and their Assignments**

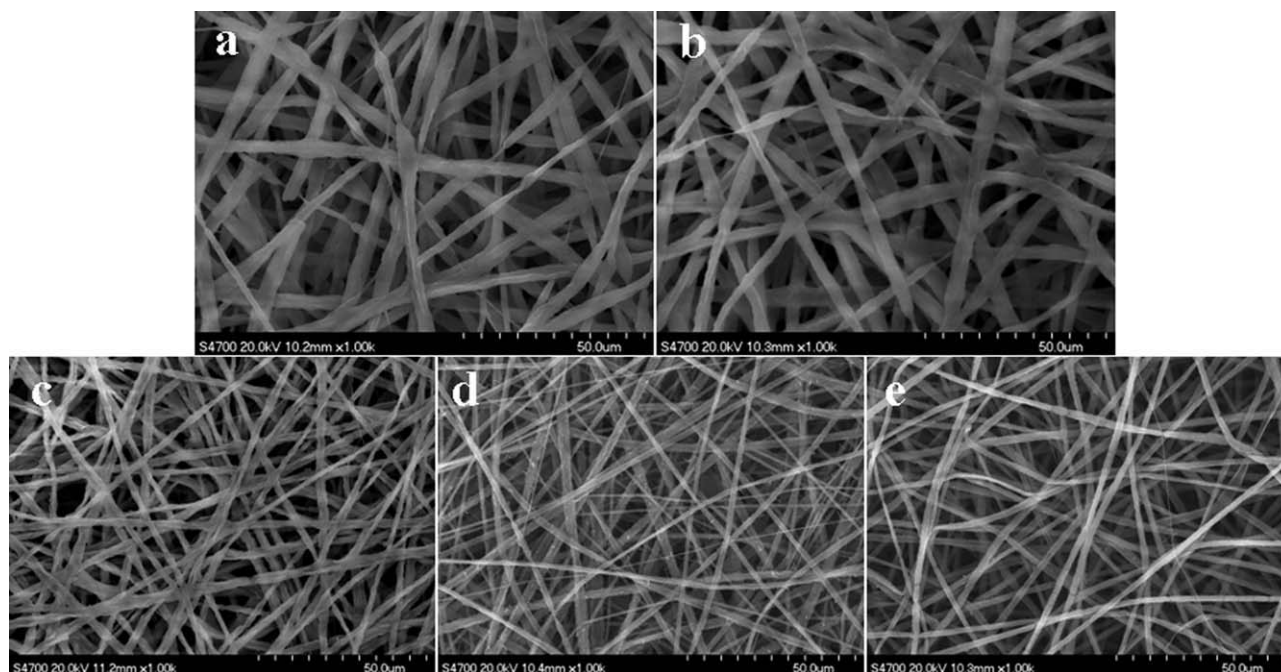| Characteristic peak (cm$^{-1}$) | Assignment | Identification |
|---|---|---|
| 3440 | Hydrogen bonding | O-CS |
| 1720 | C=O of NCOR | – |
| 1751 | C=O of OCOR | – |
| 2920, 2850 | CH$_2$ groups | – |
| 2900 | CH$_2$ stretching | PEO |
| 1455 | CH$_2$ bending | – |
| 1100 | C—O—C group | – |
| 985 | C—O—C group | – |

**Figure 2** SEM images of fibers with O-CS/PEO mass ratios: (a) 3/1, (b) 2/1, (c) 1/1, (d) 1/2, and (e) 1/3, respectively. Voltage = 22 kV, tip-to-collector distance = 15 cm, flow rate = 1.8 mL/h.

the composition of the electrospinning solution.[15] It could be found that, when O-CS/PEO = 3/1 and 2/1, the short fibers and bonded fibers was obtained, respectively, as shown in Figure 2(a,b). With an increase of PEO content, the composite fibers formation ability improved, prior to deposition on the collector, the jet showed a fluid stability which lead to formation of fine fibers. As the O-CS/PEO ratio reached up to 1/1, the bonded and short fibers disappeared, smooth and homogeneous fibers were produced [Fig. 2(c)]. When the mass ratio of O-CS/PEO increased from 1/1 to 1/3, the electrospinning process became fluent and the average diameter of the composite fibers gradually became small and uniform.

During the smooth fibers process, the relatively higher conductivity and viscosity were both favorable factors for improving electrospinnability.[13,27] Higher viscosity polymer solutions usually exhibited longer stress relaxation time, which could prevent the fracturing of ejected jets during electrospinning. Meanwhile, the high conductivity could enhance the electric force, which helped to strengthen the tensile to improve the formation of ultrafine composite fibers.[32] In this work, because the hydroxyl and amino groups on the monosaccharide structure of the chitosan were not fully acylated, an increase of O-CS content could lead to an increase in the conductivity of the solution. However, it was found that viscosities of the mixed solutions reduced greatly with increase of O-CS content and the viscosity changed from 772 mPa s (O-CS/PEO = 1/3) to 445

mPa s (O-CS/PVEO = 3/1), as shown in Figure 3. When O-CS/PEO = 3/1 and 2/1, the blend solutions could not be electrospun smoothly and continuously, because of low viscosity and high conductivity. With an increase in the PEO content, the conductivities of the solutions gradually fell, whereas the viscosities of the solutions increased high enough for fibers formation.

The electric field strength (EFS) had an effect on the average diameter of the composite fibers and their diameter distribution, as shown in Figure 4. The diameter distribution of fibers became narrow
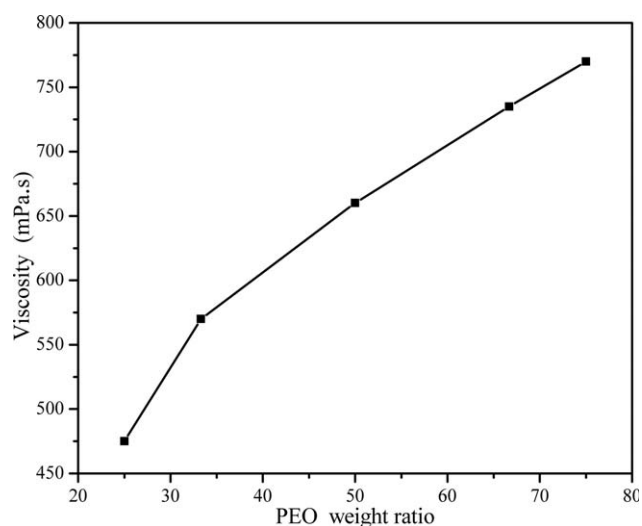


**Figure 3** Viscosities of the O-CS/PEO blend electrospinning solutions at different weight ratios.
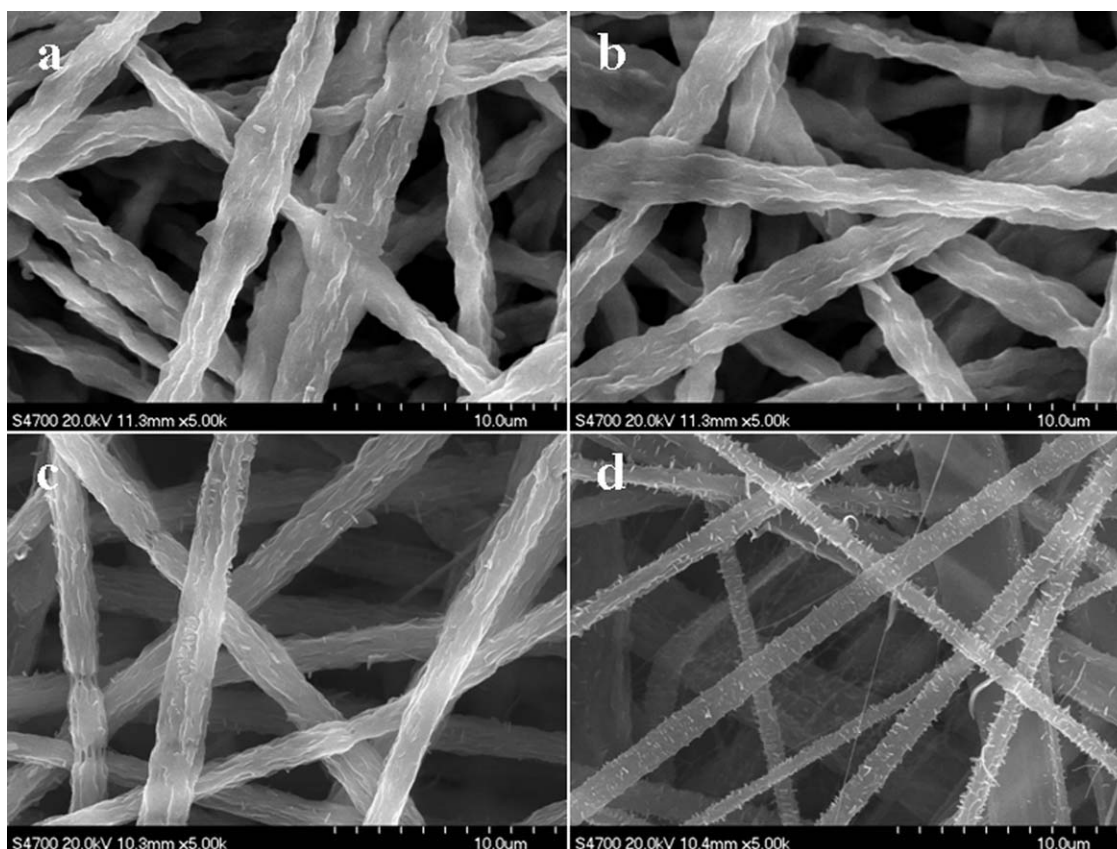
**Figure 4** SEM images of composite fibers electrospun with different applied field strength (kV): (a) 12, (b) 15, (c) 18, and (d) 21.

with increase of electrospinning voltage from 12 to 21 kV at a constant ratio (O-CS/PEO = 1/2). The static electric force was enhanced with increase of electrospinning voltage, the charge species accumulating on the surface of a pendant drop destabilizes the hemispherical shape into Taylor's cone. Beyond a critical value, a charged polymer jet is ejected from the apex of the cone, and then carried to the collective screen. Both the electrostatic and the coulombic repulsion forces are responsible for the thinning of the fibers during its trajectory to the collective screen.[8] Moreover, the rapid evaporation of the solvent was desired to prevent the development of discontinuities in the ejected jet.[33] For blend solutions, there were a critical distance (Dc), when the collection distance was smaller than Dc, electrospinning forming a stable single jet and larger sized fibers microfibers [Fig. 2(b)], when the collection distance was larger than Dc, the solvent was evaporated completely, coming into a ultrafine fibers [Fig. 2(d)].[34]

## Water contact angle

Wettability is one of the most important properties of solid surfaces which are governed by both the chemical composition and the roughness of the sur-face. Functional surfaces with special wettability play an important role in the field of biological materials. Figure 5 showed the photographs taken during WCA measurements. The electrospun O-CS/PEO composite fibers membranes revealed a quite hydrophobic character. The eletrospun O-CS/PEO composite fibers membranes with weight ratio 3/1 showed a high WCA of 130.7°. On the one hand, O-CS was organic-soluble chitosan with an intrinsic hydrophobic property; on the other hand, the O-CS altered the electric charge of electrospinning
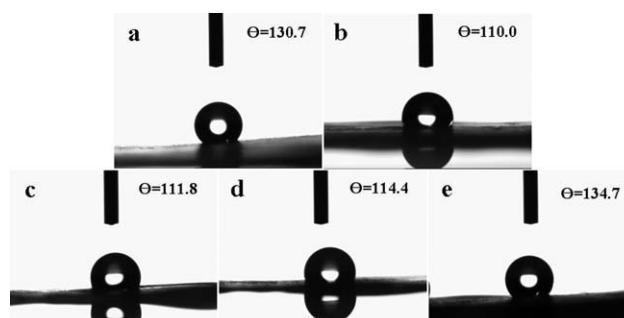


**Figure 5** WCA photographs of ultrafine composite fibers membranes with O-CS/PEO mass ratios: (a) 3/1, (b) 2/1, (c) 1/1, (d) 1/2, and (e) 1/3.
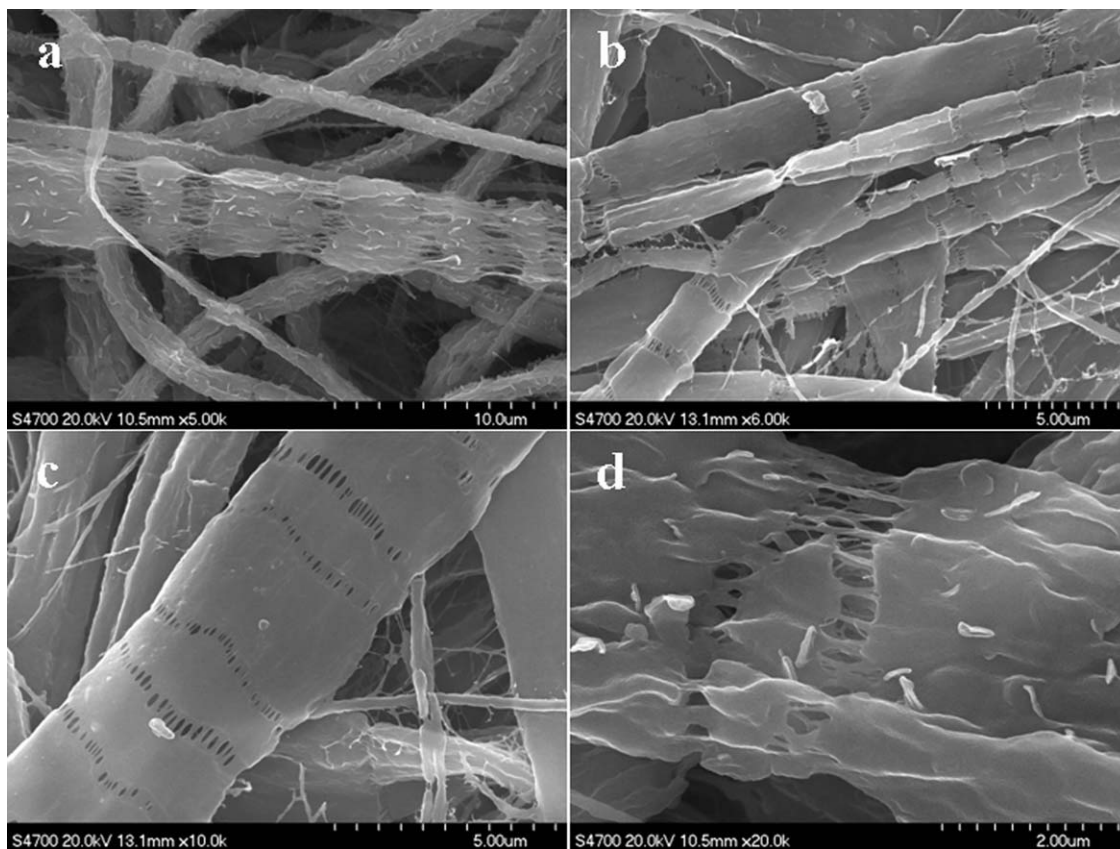
**Figure 6**   SEM images of electrospun neck and porous fibers at different magnifications.

solution, which further influenced the morphology of the composite fibers, resulting an increased hydrophobicity.[35] The addition of PEO to solutions generated a viscosity and surface tension suitable for electrospinning. However, the PEO is a linear amphiphilic polymer, as the concentration of PEO was increased, the WCA decreased down to 110.0° [Fig. 5(b)].

Both the chemical structure and rough surface morphology are the impact factors for wettability of materials. The electrospun composite fibers obtained from the O-CS/PEO solution were randomly oriented and each fiber had a rough surface morphology, large-scale grooves with a diameter of hundred nanometers were also observed on the individual fiber. Cassie and Baxter proposed an equation to describe the relationship between the WCA of a smooth surface ($\theta$) and the WCA of a rough surface ($\theta r$) composed of solid and air.

$$\cos \theta r = f_1 \cos \theta - f_2$$

In which $f_1$ and $f_2$ are the fractions of solid/water interface and air/water interface respectively, and $f_1 + f_2 = 1$. Given ($\theta$) and ($\theta r$), $f_1$ and $f_2$ could be calculated by the equation. The fibers membranes included much air between the individual electro-

spun fibers during the measurement of WCA, according to Cassie and Baxter equation, an increase in the fraction of air surface brought an increase in WCA of the surface. Then the WCA were increased up from 111.8° to 134.7° with the average diameter of the ultrafine composite fibers gradually became small and uniform [Fig. 5(c–e)].

### Neck and porous structure

The electrospun polymer solution could produce a lot of special structure. Figure 6 showed SEM photographs of a mixed pattern of neck and porous structure of electrospun composite fibers from O-CS/PEO solution. The composite fibers had a larger specific surface area, the porous size had a wide distribution from several ten to a few hundred nanometers in diameter. The neck structure might induced by the fibers which was elongated in the direction of stretching through the electric field. The porous structure was induced by phase separation, as reported by Wendorff and coworkers,[36] phase separation was the driving force of porous fibers, and thermodynamic instability was the driving force of phase separation. The polymer-rich phase formed the fiber matrix and solvent-rich phase gave rise to the porous.
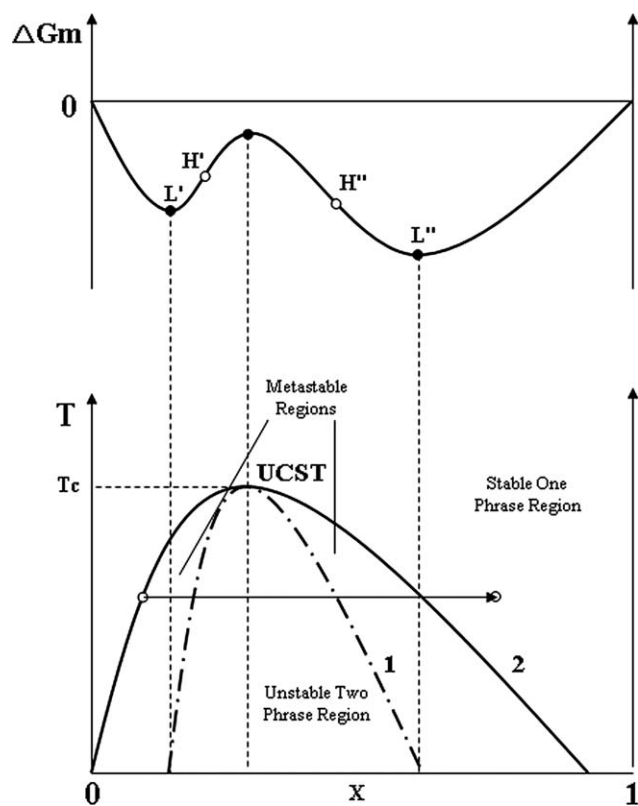
**Figure 7** The Equilibrium phase diagram with the upper critical solution temperature (UCST) and the curve between mixed Gibbs free energy ($\Delta G_m$) and consist ($x$) of blend system.

In an effort to elucidate the mechanism of porous fibers formation, a model simulation was performed.[37] The upper curve in the Figure 7 described the relationship between mixed Gibbs free energy ($\Delta G_m$) and system consists ($x$) at a certain temperature ($T_1$). In the curve, H′ point and H″ point were two inflection points, the section between H′ and H″ was the convex curve. The blend system was an unstable state in this section, the phase separation would occur. The blend system was in a metastable state between the H′ and L′ point or H″ and L″ point. If $x <$ L′ or $x >$ L″, the blend system was in a stable state. Therefore, the inflection point was the boundary conditions of unstable state (phase separation state), the unstable phase region could be calculated. The condition of inflection point appeared was as follows:

$$\partial^2 (\Delta G_m)/\partial x^2 = 0$$

The lower part of the Figure 7 was the phase diagram of the blend system at different temperatures. The Line 1 in the phase diagram was the demarcation line of unstable two phase regions and metastable region, that is, Spinodal line.[38] In this line: $\partial^2 (\Delta G_m)/\partial x^2 = 0$, The Line 2 in the phase diagram

was the demarcation line of metastable region and stable phase region. As a result, when the curve ($\Delta G_m$ to $x$) is concave, $\partial^2 (\Delta G_m)/\partial x^2 > 0$ the blend system was in stable state or metastable state; when the curve is convex, $\partial^2 (\Delta G_m)/\partial x^2 < 0$ the phase separation occurred.

Figure 7 showed an upper critical solution temperature (UCST) system. When temperature ($T$) was higher than the UCST, the system with all consist was compatible thermodynamics, on the contrary, when $T$ was lower than the UCST, the system with certain consist was compatible thermodynamics and the other consist was incompatible thermodynamics. It should be noted that most of the polymers blend systems were incompatible thermodynamics, which could separate. The morphology after the phase separation was governed by both the thermodynamics of phase separation and dynamics of the electrospinning process. Polymer droplets were caused by the local concentration fluctuations (interfacial gradient coefficient). The polymer droplets had an excessive amount of surface energy, so energy was increased as the process of polymer droplets. The activation energy produced from polymer droplets process could make the system in a metastable state cross the barrier and lead to the phase separation, and then a porous structure could be observed.[37]

The phase diagram was characterized by three distinct regions of the stable one-phase region, the unstable two-phase region, and the metastable regions. The point indicated by open circle in Figure 7 corresponded to the initial concentration of the polymer and the arrow indicated how the system traversed along the concentration axis with continued solvent evaporation. A phase separation could be seen in a system undergoing solvent evaporation, in which polymer concentration increased gradually which pushed the system to traverse across the phase diagram. The polymer concentration increased in the direction indicated by the arrow as a result of solvent evaporation and the system traversed across the phase diagram from the single phase region to the metastable region where polymer droplets could be discerned. With further increase of the polymer concentration, the droplet morphology transforms into an interconnected structure in the unstable region. This morphology further transformed into porous structure as the system enters the polymer-rich metastable region.[39]

## CONCLUSIONS

The FTIR results confirmed that ultrafine composite fibers membranes were composed of O-CS and PEO. A significant decrease in the diameter of electrospun O-CS/PEO composite fibers with increase of the PEO content was observed. At the same time, the

increase of the EFS and collection distance also could lead to the decrease of the diameter of composite fibers. The photographs taken during WCA measurements revealed a quite hydrophobic character, the value of WCA was decided by the O-CS, PEO, and the fiber membrane structure together. There were a number of mixed patterns of neck and porous structure fibers appeared during electrospinning. A phase diagram theoretical model was performed to explain the formation mechanism of porous structure.

## References

1. Wongsasulak, S.; Kit, K. M.; Mcclements, D. J.; Yoovidhya, T.; Weiss, J. Polymer 2007, 48, 448.
2. Reneker, D. H.; Chun, I. Nanotechnology 1996, 7, 216.
3. Kenawy, E. R.; Bowlin, G. L.; Mansfield, K.; Layman, J.; Simpson, D. G.; Sanders, E. H.; Wnek, G. E. J Controlled Release 2002, 81, 57.
4. Deitzel, J. M.; Kleinmeyer, J.; Harris, D.; Beck Tan, N. C. Polymer 2001, 42, 261.
5. Schultz, J. M.; Hsiao, B. S.; Samon, J. M. Polymer 2000, 41, 8887.
6. Lopes, P. E.; Ellison, M. S.; Pennington, W. T. Plast Rubber Compos 2006, 35, 294.
7. Wongsasulak, S. Ph.D. Thesis, University of King Mongkut's University of Technology Thonburi, Thailand, 2005.
8. Zhang, Y. Z.; Venugopal, J.; Huang, Z. M.; Lim, C. T.; Ramakrishna, S. Polymer 2006, 47, 2911.
9. Stylianopoulos, T.; Bashur, C. A.; Goldstein, A. S.; Guelcher, S. A.; Barocas, V. H. J Mech Behav Biomed Mater 2008, 1, 326.
10. Gibson, P.; Schreuder-Gibson, H.; Rivin, D. Colloids Surf A: Physicochem Eng Aspects 2001, 187, 469.
11. Casper, C. L.; Stephens, J. S.; Tassi, N. G.; Chase, D. B.; Rabolt, J. F. Macromolecules 2004, 37, 573.
12. Liaoa, S.; Murugan, R.; Chan, C. K.; Ramakrishna, S. J Mech Behav Biomed Mater 2008, 1, 252.
13. Fong, H.; Chun, I.; Reneker, D. H. Polymer 1999, 40, 4585.
14. Deitzel, J. M.; Kleinmeyer, J. D.; Hirvonen, J. K.; Beck Tan, N. C. Polymer 2001, 42, 8163.
15. Zhang, C. X.; Yuan, X. Y.; Wu, L. L.; Han, Y.; Sheng, J. Eur Polym J 2005, 41, 423.
16. Gupta, K. C.; Ravi Kumar, M. N. V. Polym Int 2000, 49, 141.
17. Risbud, M.; Hardikar, A.; Bhonde, R. Cell Trans 2000, 9, 25.
18. Risbud, M. V.; Hardikar, A. A.; Bhat, S. V.; Bhonde, R. R. J Controlled Release 2000, 68, 23.
19. Sechriest, V. F.; Miao, Y. J.; Niyibizi, C.; Werterhausen-Larson, A.; Matthew, H. W.; Evans, C. H.; Fu, F. H.; Suh, J. K. J Biomed Mater Res 2000, 49, 534.
20. Montembault, A.; Tahiri, K.; Korwin-Zmijowska, C.; Corvol, T.; Domard, A. Biochimie 2006, 88, 551.
21. Muzzarelli, R.; Biagini, G.; Pugnaloni, A.; Filipini, O.; Baldassarre, V.; Castaldini, C.; Rizzoli, C. Biomaterials 1989, 10, 598.
22. Desai, K.; Kit, K.; Li, J.; Zivanovic, S. Biomacromolecules 2008, 9, 1000.
23. Son, W. K.; Youk, J. H.; Lee, T. S.; Park, W. H. Polymer 2004, 45, 2959.
24. Yoon, K.; Kim, K.; Wang, X. F.; Fang, D. F.; Hsiao, B. S.; Chu, B. Polymer 2006, 47, 2434.
25. Park, W. H.; Jeong, L.; Yoo, D. I.; Hudson, S. Polymer 2004, 45, 7151.
26. Zong, Z.; Kimura, Y.; Takahashi, M.; Yamane, H. Polymer 2000, 41, 899.
27. Theron, S. A.; Zussman, E.; Yarin, A. L. Polymer 2004, 45, 2017.
28. Ma, G. P.; Yang, D. Z.; Kennedy, J. F.; Nie, J. Carbohydr Polym 2009, 75, 390.
29. Duan, B.; Dong, C.; Yuan, X.; Yao, K. J. Biomater Sci: Polym Ed 2004, 15, 797.
30. Jackson, M.; Haris, P. I.; Chapman, D. J. Mol Struct 1989, 214, 329.
31. Ngarize, S.; Adams, A.; Howell, N. K. Food Hydrocolloids 2004, 18, 49.
32. Li, J. X.; He, A. H.; Zheng, J. F.; Han, C. C. Biomacromolecules 2006, 7, 2243.
33. Shenoy, S. L.; Bates, W. D.; Frisch, H. L.; Wnek, G. E. Polymer 2005, 46, 3372.
34. Zhang, Y. Z.; Su, B.; Ramakrishna, S.; Lim, C. T. Biomacromolecules 2008, 9, 136.
35. Lu, X. B.; Zhou, J. H.; Zhao, Y. H.; Qiu, Y.; Li, J. H. Chem Mater 2008, 20, 3420.
36. Bognitzki, M.; Czado, W.; Frese, T.; Schaper, A.; Hellwig, M.; Steinhart, M.; Greiner, A.; Wendorff, J. H. Adv Mater 2001, 13, 70.
37. Dayal, P.; Liu, J.; Kumar, S.; Kyu, T. Macromolecules 2007, 40, 7689.
38. Bruder, F.; Brenn, R. Phys Rev Lett 1992, 69, 624.
39. Guenthner, A. J.; Khombhongse, S.; Liu, W. X.; Dayal, P.; Reneker, D. H.; Kyu, T. Macromol Theory Simul 2006, 15, 87.